ACS OMEGA

http://pubs.acs.org/journal/acsodf

Article

Synthesis and Photophysical, Electrochemical, and DFT Studies of Piperidyl and Pyrrolidinyl Chalcones

Humera Baig, Amber Iqbal, Alvina Rasool, Syed Zajif Hussain, Javed Iqbal, Meshari Alazmi, Nawaf Alshammari, Amira Alazmi, Amer AlGhadhban, Abdel Moneim E. Sulieman, Kamaleldin B. Said, Habib-ur Rehman, and Rahman Shah Zaib Saleem*

Cite This: *ACS Omega* 2023, 8, 28499−28510

Read Online

ACCESS | Metrics & More | Article Recommendations | Supporting Information

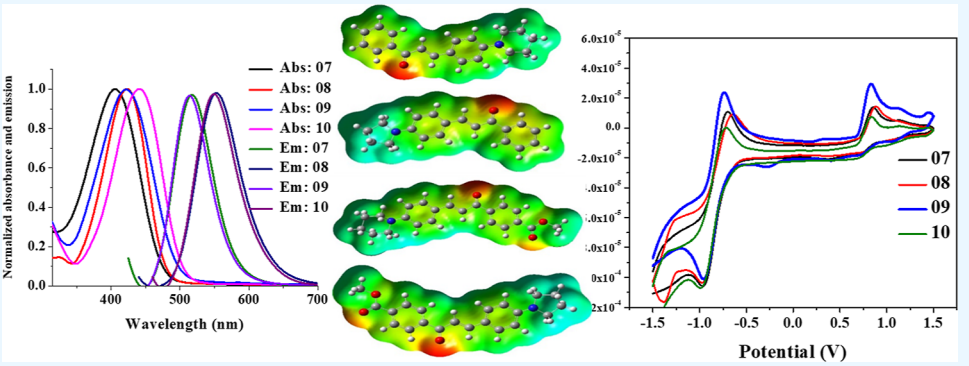

ABSTRACT: Small organic molecules with interesting optical and electrochemical properties find applications as organic luminescent materials. In this work, we report the synthesis of novel chalcones with D−A−D and D−A−D−A architecture, followed by their optical, electrochemical, and computational studies. The absorption band of these compounds occurs at 360−480 nm with emission maxima appearing around 513−552 nm. The large Stokes shifts ($\Delta\lambda$) for all compounds (90−132 nm) suggest intramolecular charge transfer (ICT) in the excited states. The molar absorptivity and fluorescence quantum yields were found to be in the range of 1.7−4.26 × 10^4 M^{-1} cm^{-1} and 0.29−0.39, respectively. The electrochemical parameters were determined by using cyclic voltammetry (CV). Density functional theory (DFT) calculations of all compounds were made by using B3LYP/G (d,p) functionals in chloroform and were found to have a good correlation with experimental results. Preliminary studies of absorption, photoluminescence, CV, and their theoretical correlation suggest that these compounds may be optimized for their applications in optoelectronics, sensing, and bioimaging.

INTRODUCTION

The pioneering work of Tang and Slyke has led to an immense interest in organic luminescent compounds.[1−5] In the last three decades, these materials have found their applications in various areas including organic light-emitting devices,[6−9] fluorescent probes,[10,11] photovoltaics,[12,13] electroluminescent materials for organic electronics,[14] and transistor devices.[15,16] Among these materials, chalcones exhibiting intramolecular charge transfer (ICT) characteristics have been shown to carry interesting photophysical and photochemical properties.[17] These properties make chalcones particularly interesting, considering the small Stokes shifts of many commonly used fluorescent compounds like fluorescein (24 nm), 5-carboxy-fluorescein (36 nm), fluorescein isothiocyanate (24 nm), rhodamine (26 nm), rhodamine 6G (24 nm), Rhodamine Green (26 nm), Cy2 (13 nm), Nile red (70 nm), BODIPY 493 (10 nm), BODIPY 505 (10 nm), MitoTracker Green (26 nm), and MitoTracker Red (20 nm).[18] Chalcones constitute a large class of organic compounds that have two aromatic rings connected via a ketoethylenic group.[19] Their structure provides high delocalization of the pi-electrons. The ease of synthesis makes them excellent scaffolds to construct novel derivatives for subsequent evaluation of optical properties.[20−22] Thus, besides their wide-ranging medicinal properties,[23−35] chalcones have been studied for optoelectronic devices,[36] electrochemical materials,[37] as fluorescent and chromophoric sensors for metallic ions,[38] nonlinear optical materials,[39] and dye-sensitized solar cells.[40]

Received: April 24, 2023
Accepted: July 18, 2023
Published: July 27, 2023

Scheme 1. General Procedure for the Synthesis of Compounds

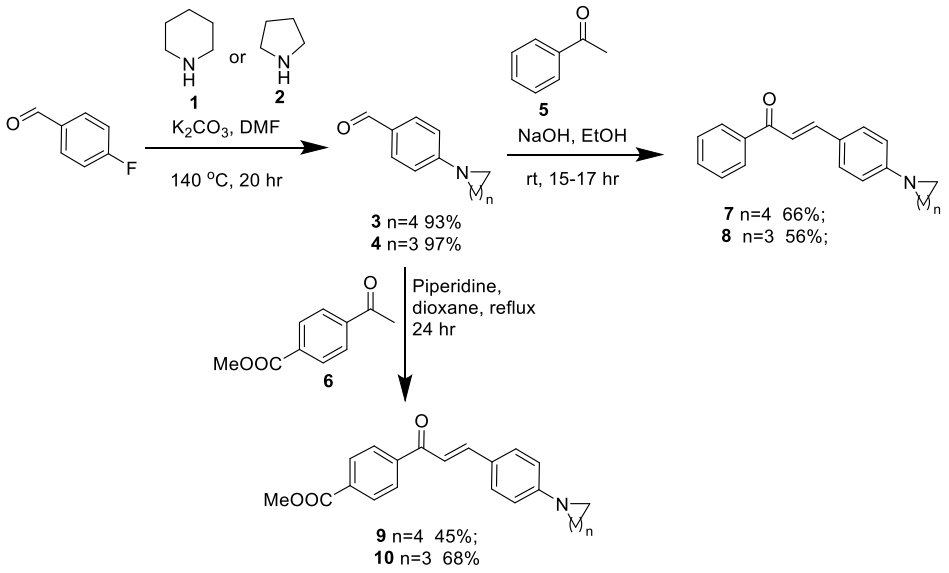

With an interest to explore the photophysical characteristics of organic scaffolds,[41,42] in the current work, we present the synthesis of novel chalcones carrying an electron-donating piperidyl or pyrrolidinyl ring on ring B and no substituent on ring A (making it a D−A−D architecture) or an ester on ring A (making it a D−A−D−A architecture). Then, we present experimental and theoretical studies of these chalcones including UV−vis absorbance, photoluminescence (PL), analysis of highest occupied molecular orbital (HOMO)/lowest unoccupied molecular orbital (LUMO) energy level, density of state (DOS) analysis, molecular electrostatic potential (MEP) surface analysis, transition density matrix (TDM), exciton binding energy (E_b), and reorganization energy (RE).

RESULTS AND DISCUSSION

Chemistry. The synthesis of the compounds involved the aromatic nucleophilic substitution reaction of 4-fluorobenzaldehyde with piperidine (**1**) and pyrrolidine (**2**) to yield compounds **3** and **4**, respectively. These compounds were then subjected to the Claisen−Schmidt condensation presented in Scheme 1. Compounds **7** and **8** were prepared by reacting compounds **3** and **4** with acetophenone (**5**) in ethanol using an aqueous solution of sodium hydroxide. The mixture was stirred for 15−17 h at room temperature. For compounds **9** and **10**, methyl-4-acetylbenzoate (**6**) was refluxed for 24 h with compounds **11** and **12** using piperidine as a catalyst. The purification of the crude products was done via column chromatography. The yields were in the range of 45−68%, and their structures were established using ^{1}H NMR, ^{13}C NMR, IR, and mass spectrometry. The values of coupling constants revealed the formation of *E*-isomers.

UV−Visible Absorption and Emission Properties. The UV−vis absorption and emission spectra, obtained in different solvents, are shown in Figures 1 and 2. The corresponding spectral data (λ_{max}^{abs}, λ_{max}^{em}, and Δ) is presented in Table 1. To probe the solvent polarity effect (solvatochromism), the absorption and emission spectra of compounds **07−10** were obtained in a polar protic solvent (ethanol), a polar aprotic solvent (acetonitrile), and a nonpolar solvent (chloroform) at a concentration of 1×10^{-5} M. The absorption spectra of the chalcones exhibited two distinct absorption bands in all the three solvents. The absorption band centered at the lower wavelength (240−280 nm) corresponds to localized $\pi-\pi^*$ transitions in the ketoethylenic group, while the low energy band (360−480 nm) is attributed to delocalized $\pi-\pi^*$ electronic transition or ICT.

Comparing the effect of having pyrrolidine and piperidine rings as donating groups on the photophysical properties of compounds **7−10**, the pyrrolidine ring pyrrolidine acts as a better electron density pushing group. For example, in chloroform, compounds **8** (λ_{abs}^{exp} = 423) and **10** (λ_{abs}^{exp} = 440) have red-shifts of 18 and 20 nm as compared to the piperidine-containing counterparts **7** (λ_{abs}^{exp} = 405) and **9** (λ_{abs}^{exp} = 420), respectively. A similar trend is also observed in CAN and EtOH. In the other cross-comparison of compounds **9** and **10** carrying −COOMe with compounds **7** and **8**, compounds **9** and **10** are red-shifted by 15 and 27 nm in chloroform. This bathochromic shift is attributed to the electron-withdrawing nature of ester linkage, which pulls e^- density toward itself giving a D−A−D−A architecture to compounds **9** and **10**.

The polarity-driven red shifts from acetonitrile to ethanol ($\Delta\lambda_{abs}$) ranged from 7 to 13 nm. These small solvatochromic effects suggest that there is no significant ICT in the ground state.[20] The PL spectra of these compounds in chloroform, acetonitrile, and ethanol (1×10^{-5} M) were recorded at respective absorption maxima (λ_{max}). The PL maxima of these chalcones showed strong green fluorescence (513−552 nm) in chloroform and ethanol (545−568 nm). The intensities of PL of compounds **9** and **10** in acetonitrile and of all compounds in ethanol are remarkably low due to dipole−dipole interaction and hydrogen bonding.[17] Importantly, the Stokes shifts for compounds **7−10** were calculated from the difference between the absorption maxima and emission maxima values in chloroform and found to be 111, 90, 132, and 108 nm, respectively. Similarly, the Stokes shift values were found to be 138, 114, 139, and 118 nm, respectively, for compounds **07−10** in ethanol. The appreciable Stokes shifts values of these compounds seem to arise from the ICT from the donor pyrrolidine and piperidine group to the ketoethylenic acceptor moiety in the excited state through π-extended conjugation. The high Stokes shift values make these compounds good hits

https://doi.org/10.1021/acsomega.3c02813
ACS Omega 2023, 8, 28499−28510

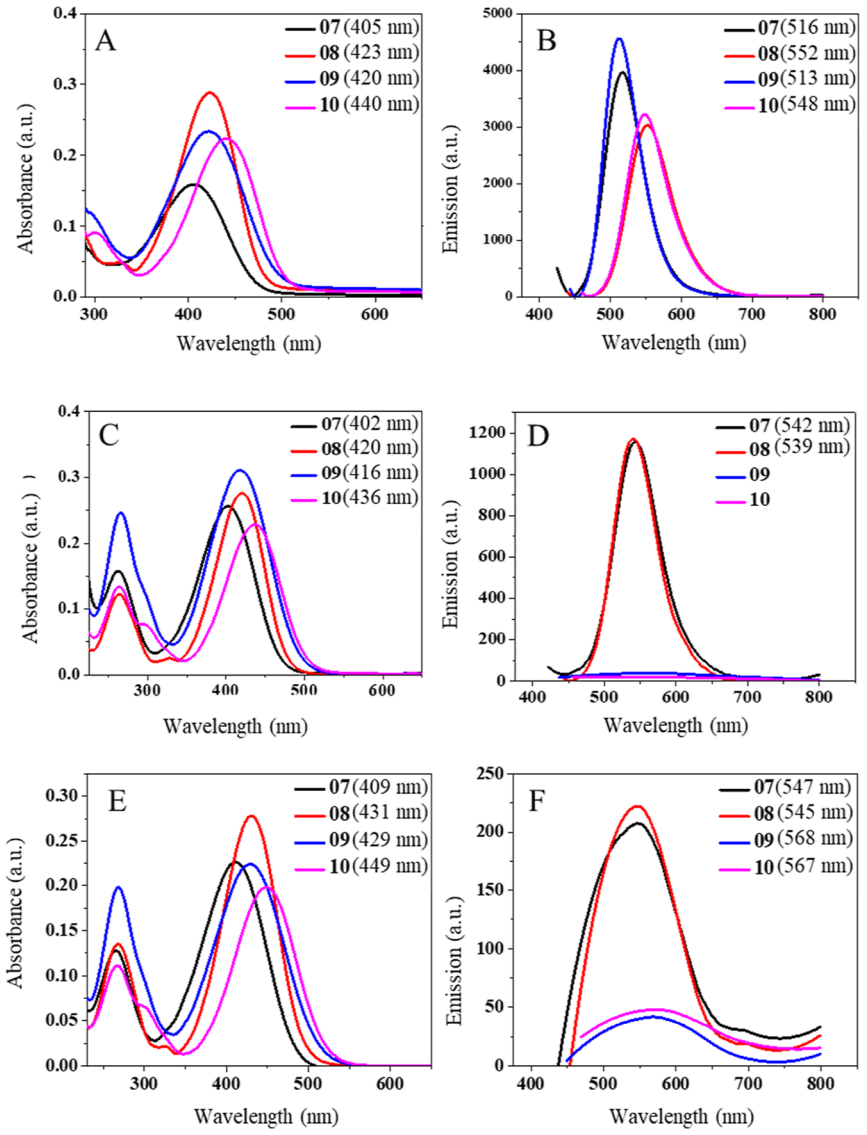

Figure 1. Absorption and emission spectra of chalcones **7**−**10** [(A) absorption spectra in chloroform, (B) emission spectra in chloroform, (C) absorption spectra in acetonitrile, (D) emission spectra in acetonitrile, (E) absorption spectra in ethanol, and (F) emission spectra in ethanol].

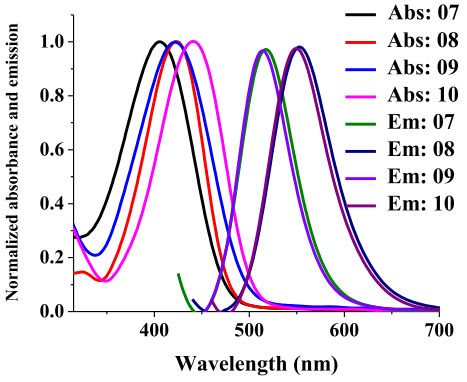

Figure 2. Normalized absorption and emission spectra of compounds **7**−**10** in chloroform.

for further studies as new fluorescent compounds with lower reabsorption of a photon in organic fluorophores and reduced self-quenching.

The molar absorptivity of compounds **07**−**10** was found to be 1.7×10^4, 4.26×10^4, 2.55×10^4, and 2.63×10^4 M^{-1} cm^{-1} (Figures S1−S8, Supporting Information), respectively, as shown in Table 2. The fluorescence quantum yields of these compounds were found to be 0.39, 0.34, 0.29, and 0.39 (Figures S9−S23, Supporting Information) in chloroform at room temperature. The low values of φ_f may be linked to the nonradiative decays, i.e., internal conversion and vibrational relaxation.

Electrochemical Properties. The electrochemical properties of compounds **7**−**10** were probed using cyclic voltammetry (CV) analysis. The cyclic voltammograms are shown in Figure 3, and the corresponding electrochemical data is summarized in Table 3. All compounds exhibit a reversible redox process, which indicates their potential for effective hole/electron transport. The HOMO energy levels of compounds **7**−**10** were found to be −5.18, −5.14, −5.18, and −5.15 eV, respectively. Compounds **8** and **10** were found to exhibit smaller ionization potential energies as compared to compounds **7** and **9** owing to the presence of pyrrolidine as an electron-donating moiety. The LUMO energy levels of

https://doi.org/10.1021/acsomega.3c02813
ACS Omega 2023, 8, 28499−28510

Table 1. Absorption and Emission Data of Chalcones 7−10[a]

	λ_{abs} nm				λ_{em} nm				$\Delta\lambda_{st}$	
compound	ACN	$CHCl_3$	EtOH	$\Delta\lambda_{abs}$	ACN	$CHCl_3$	EtOH	$\Delta\lambda_{em}$	$CHCl_3$	EtOH
7	402	405	409	07	542	516	547	31	111	138
8	420	423	431	11	539	513	545	32	90	114
9	416	420	429	13		552	568	16	132	139
10	436	440	449	13		548	567	19	108	118

[a] λ_{abs}: absorption maxima (nm), $\Delta\lambda_{abs}$: solvatochromism in the ground state, $\Delta\lambda_{em}$: emission maxima, $\Delta\lambda_{em}$: solvatochromism in the excited state, $\Delta\lambda_{st}$: Stokes shifts.

Table 2. Photophysical Parameters of Chalcones 7−10

		photophysical properties						
compound	solvent	λ_{abs}/nm	λ_{em}/nm	λ_{onset}/nm	$\Delta\lambda$/nm	E_{0-0} (eV)	ε ($M^{-1}cm^{-1}$)	φ_f
7	chloroform	405	516	472	111	2.63	1.7×10^4	0.39
8	chloroform	423	513	484	90	2.56	4.2×10^4	0.34
9	chloroform	420	552	500	132	2.48	2.5×10^4	0.29
10	chloroform	440	548	504	108	2.46	2.6×10^4	0.39

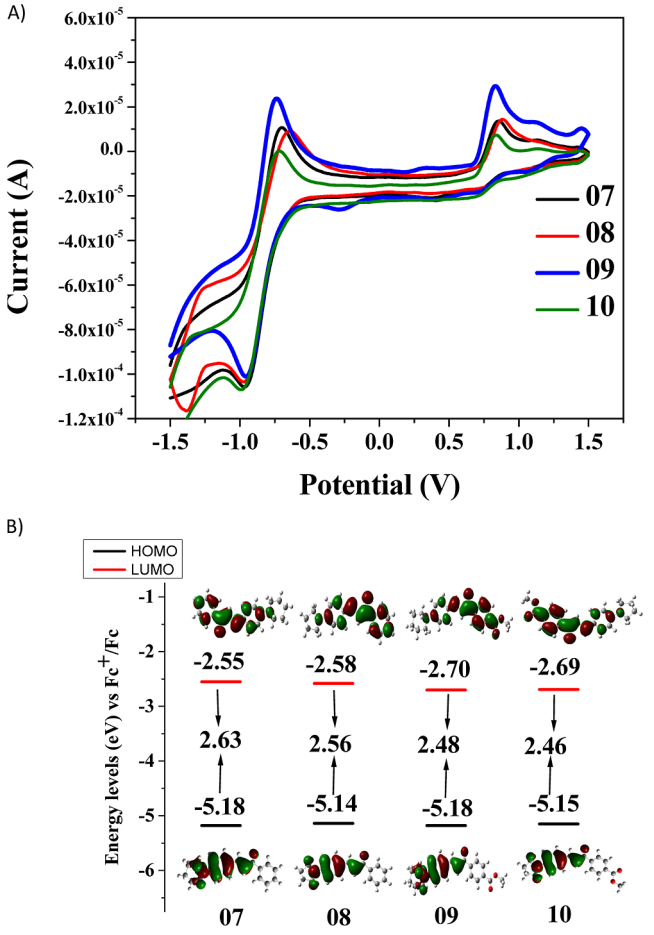

Figure 3. CV of compounds **07−10**. (A) Cyclic voltammograms of chalcones **7−10** in acetonitrile. The electrochemical analysis was performed on a CHI 660E workstation using a three-electrode cell system at room temperature in a solution of tetrabutylammonium hexafluorophosphate (nBu4NPF6) 0.1 M as a supporting electrolyte in anhydrous acetonitrile at a scan rate of 100 mV s^{-1} between voltage ranges −1.5 and 1.5 V. (B) Energy gap diagram of chalcones **7−10**.

compounds **07−10** were found to be −2.55, −2.58, −2.70, and −2.69, respectively.

Table 3. HOMO, LUMO, and Band Gap of 7−10 Calculated by CV Analysis

compound	HOMO (eV)	LUMO (eV)	E_{0-0}	λ_{onset}
7	−5.18	−2.55	2.63	472
8	−5.14	−2.58	2.56	484
9	−5.18	−2.70	2.48	500
10	−5.15	−2.69	2.46	504

UV−Visible Spectral Analysis. To deduce a suitable method, the geometries of all compounds were optimized with CAM-B3LYP,[43] MPW1PW91,[44] WB97XD,[45] and B3LYP.[46] The B3LYP at 6-31G (d, p) basis set was found to better compare well with the experimental values and was then used for all theoretical calculations (Table 4). The maximum absorption of all molecules in the gaseous and solvent (chloroform) phase was obtained by using TD-density functional theory (DFT) and IEFPCM (integral equation formalism polarizable continuum model) solvation model, respectively, and the absorption spectra are shown in Figure 4.

The study of photophysical properties was accomplished with the computations of various parameters like the symmetry of molecules, absorption maximum, the energy of excitation (ΔE), oscillator strength (f_o), LHE (light harvesting efficiency), percentage coefficient of interaction (C.I. %), and transition of molecular systems from HOMO to LUMO (Table 5). We observed that all compounds had a higher gas-phase excitation energy value than in solvent, suggesting good solubility in chloroform.

Structural Optimization and FMO Analysis. The ground-state configuration has a substantial influence on the optoelectronic properties of molecular systems, so ground-state geometry optimization was performed to calculate different geometrical constraints. All compounds were optimized at their ground state using B3LYP and 6-31G(d,p) basis sets to obtain the global minima shown in Figure 5. These compounds are suggested to have planar conformations, and the NMR studies have suggested these to be E-chalcones.

The HOMO is majorly localized in the donor region and minorly over the acceptor region, while the LUMO electronic population is majorly dispersed over the acceptor region. Table 6 represents the FMO analysis results. The HOMO/LUMO energy levels calculated for compounds **7−10** were found to be

https://doi.org/10.1021/acsomega.3c02813
ACS Omega 2023, 8, 28499−28510

Table 4. Comparison of Experimental and Theoretical λ_{max} for Chalcones 7−10

Compounds	solvent	λ_{max}^{exp} (nm)	B3LYP (nm)	CAMB3LYP (nm)	MPW1PW91 (nm)	WB97XD (nm)
7	chloroform	405	410	336	390	328
8	chloroform	423	417	350	400	344
9	chloroform	420	446	349	523	340
10	chloroform	440	458	362	534	353

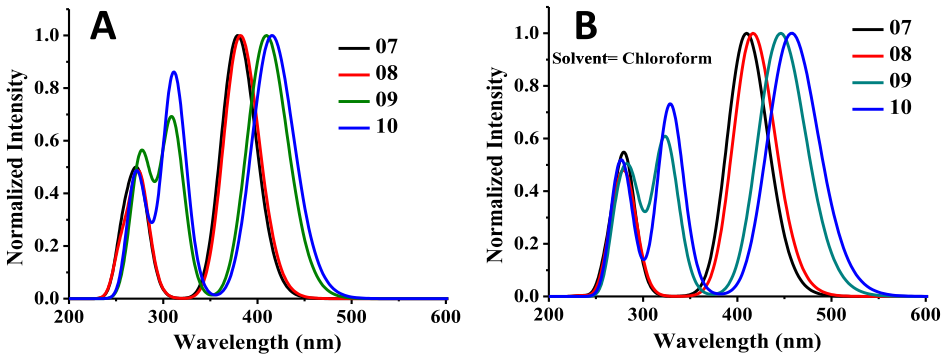

Figure 4. Theoretical absorption profile of chalcones **7−10** [(A) in gas phase and (B) in chloroform].

Table 5. Theoretical Absorption Profile of Chalcones 7−10 in the Gas Phase and Chloroform

		gas phase			chloroform				
molecules	λ_{max}^{exp} (nm)	λ_{max}^{cal} (nm)	E (eV)	f	major molecular transitions	λ_{max}^{cal} (nm)	E (eV)	F	major molecular transitions
7	405	378	3.29	0.42	H → L (48%)	410	3.02	0.91	H → L (70%)
8	423	381	3.24	0.81	H → L (69%)	417	2.97	0.98	H → L (70%)
9	420	409	3.03	0.65	H → L (70%)	446	2.78	0.75	H → L (70%)
10	440	415	2.98	0.64	H → L (90%)	458	2.71	0.75	H → L (70%)

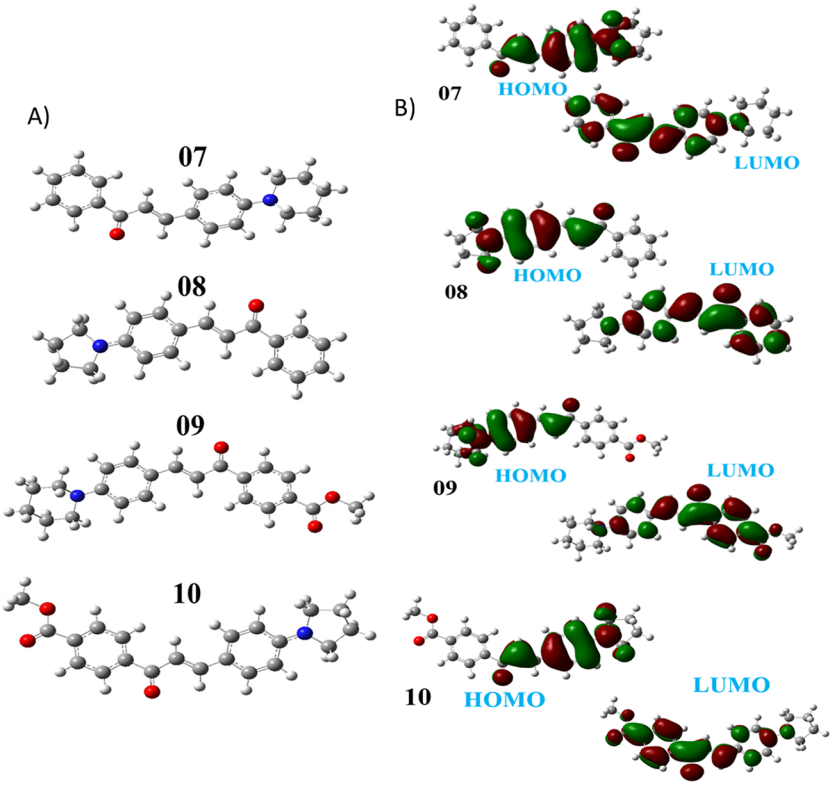

Figure 5. A) Optimized geometry of compounds **7−10** and (B) frontier molecular orbitals (FMOs) of chalcones **7−10**.

in good agreement with the experimental HOMO/LUMO energy levels obtained from CV analysis.

DOS Analysis. DOS analysis of quantum mechanics explains the presence of energy states, for the transition of

https://doi.org/10.1021/acsomega.3c02813
ACS Omega 2023, 8, 28499−28510

Table 6. Theoretically Calculated HOMO and LUMO Energies and Band Gaps (E_g) of Chalcones 7−10

molecules	HOMO (eV)	LUMO (eV)	E_g (eV)
7	−5.29	−1.80	3.49
8	−5.09	−1.66	3.43
9	−5.36	−2.09	3.27
10	−5.19	−1.98	3.21

current, in per unit energy level increments. The DOS plots show total energy states as an area underneath the peaks of the spectrum. The molecular orbital energy values are shown on the *x*-axis of the DOS diagrams. The *y*-axis shows the relative strength of states. The DOS curve plots of **07−10** presented in Figure 6 show that HOMO and LUMO are primarily contributed by the donor and minorly by the acceptor portion, and there is a good agreement of the band gap with the band gap calculated using CV studies.

MEP Surface Analysis. Electrostatic potential (ESP) analysis was carried out using the B3LYP/6-31G(d,p) functional to examine the dissemination of electrostatic charge on different parts of the compounds. ESP evaluation provides information about the relocation of charge from the donor component to the acceptor part as well as the reactivity of chromophores by highlighting the electronegative and electropositive regions. The GaussView software package was used to generate the ESP diagrams as shown in Figure 7. The multiple-hued images showed different colors from red demonstrating the highest negative potential to blue exhibiting the highest positive potential, while green hue representing the neutral region with zero potential. The red-tinted parts having high electron density are susceptible to electrophiles, while the blue-dyed zones having the least electron density are exposed to nucleophiles. These compounds understandably gave red hues in the carbonyl and ester regions, while blue hues in the regions of pyridine and pyrrolidine rings.

TDM Analysis. Multiwfn software was used to explore the electronic excitation including interaction in the molecule at an excited state by using TDM analysis.[47] In TDM graphs, the molecules are fragmented into two components: donor (D) and acceptor (A). The molecules, as shown in Figure 8, have a uniform charge distribution and charge coherency in the acceptor area, implying good charge transmission from donor to acceptor.

Charge-Transfer Integral. The charge-transfer integral illustrates internal stacking in a molecule and symbolizes the ease of charge transport. Higher charge integral values indicate that the charge mobility route has fewer anomalous states. The charge integral values were determined by using the following equations.[48,49]

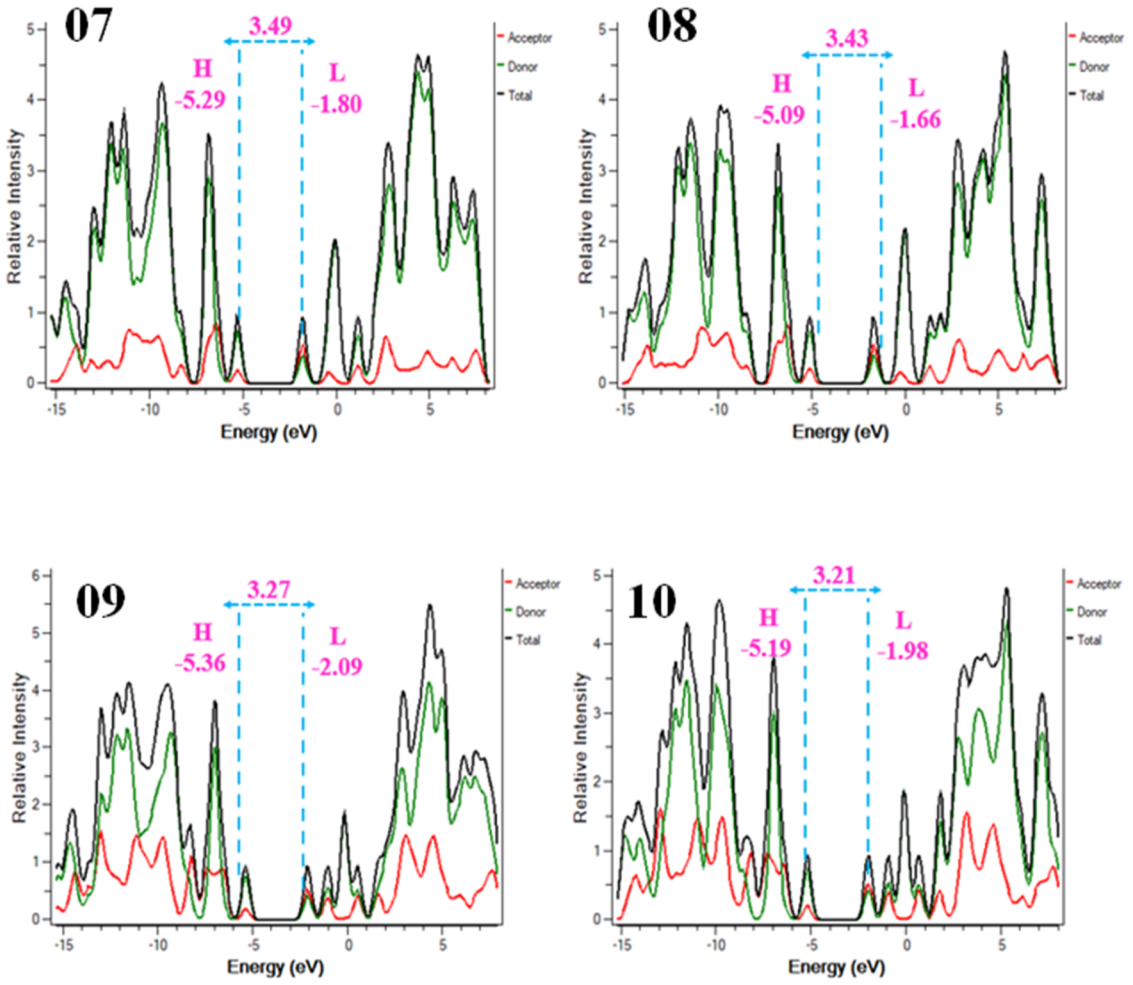

Figure 6. DOS analysis of compounds **7−10**.

https://doi.org/10.1021/acsomega.3c02813
ACS Omega 2023, 8, 28499−28510

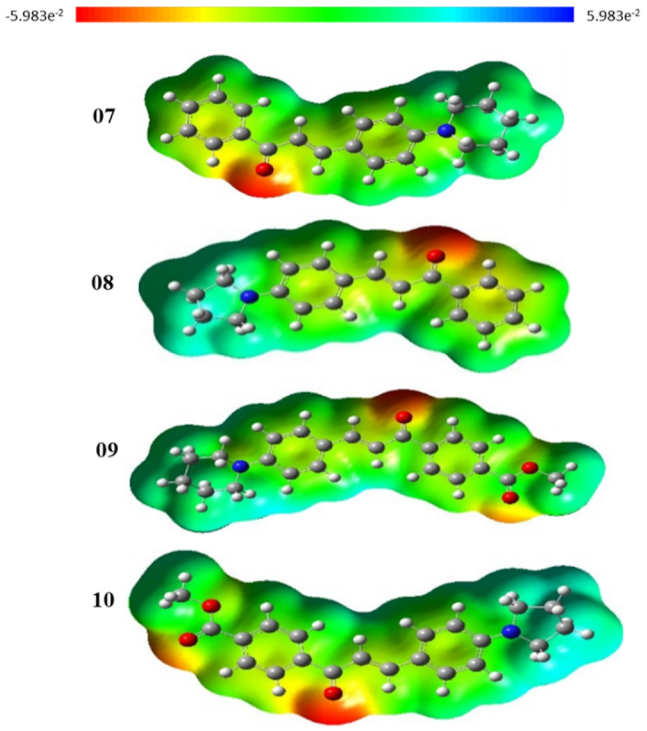

Figure 7. MEP plots of compounds **7**−**10**.

$$t_h = \frac{1}{2}(E_H - E_{H-1})$$

$$t_e = \frac{1}{2}(E_{L+1} - E_L)$$

where E_H and E_L are the energies of HOMO and LUMO in eV, E_{H-1} is the energy of orbital one lower than HOMO, and E_{L+1} is the energy of orbital one next to LUMO.

Table 7 displays the transfer integral of electrons (t_e) and holes (t_h) and shows a better electron mobility rate for compound **7** and compound **8** and a better hole movement capability for compound **10**.

Dipole Moment. The smooth texture of the donor−acceptor blend layer in solar devices is intimately related to the solubility of the molecule, and generally, the dipole moment value is a good indicator for the solubility. The dipole moment of all compounds was calculated in the ground and excited states at the mentioned DFT functional, and values have been tabulated in Table 8, demonstrating that these compounds have good solubility in chloroform solvent.

CONCLUSIONS

In the current work, we have reported the synthesis of novel chalcone derivatives. These chalcones were yellow to brown with absorption bands occurring at 360−480 nm and emission bands at 513−552 nm. The absorption and emission (λ_{abs} and λ_{em}) maxima were determined in different solvents to study solvatochromism. The minor red shifts were observed in absorption maxima, while increasing polarity from chloroform to ethanol suggests no significant ICT at the ground state. All compounds exhibited PL with high intensity in chloroform. However, in ethanol, the emission is negligible probably due to the hydrogen bonding between the solute and solvent molecules. Importantly, these compounds have shown large Stokes shift values of 90−132 nm. The HOMO/LUMO energy levels and band gaps of compounds **08** and **10** bearing pyrrolidine at the para position of ring B are lower than those of compounds **07** and **09** with piperidine, suggesting better donating abilities of the pyrrolidine ring. All compounds displayed appreciable fluorescence quantum yields (φ_f) ranging from 0.29 to 0.39. Furthermore, the DFT studies including molecular geometry, FMO analysis, reorganization energies, dipole moments, and UV−vis analysis are presented in this work and match well with the experimental results. The facile synthesis and appreciable preliminary properties present the potential of these compounds for further studies to optimize these for application in organic electronics and fluorescent-based probes for bioimaging.

MATERIALS AND METHODS

Chemistry. All chemicals were purchased from Sigma-Aldrich or TCI and were 98−100% pure. Solvents (*n*-hexane, ethyl acetate, and dichloromethane) were purchased from local vendors and purified by distillation before use. ^{1}H and ^{13}C NMR spectra were recorded with a BRUKER AVANCE Neo spectrometer (600 MHz). Chemical shifts and coupling constants (J) were reported in ppm and Hz, respectively. A BRUKER ALPHA platinum ATR spectrophotometer was used to obtain the IR spectra of compounds. GCMS data was recorded on a Thermo Scientific ISQ Trace 1300 GC−MS with an AI 1310 Autosampler. A micro-TOF mass spectrometer was used to determine HRMS. The Stuart SMP3 apparatus was used to determine the melting points. UV studies were performed on the SHIMADZU UV-1800 spectrophotometer at room temperature by using glass cuvettes. A Perkin Elmer multimode plate spectrophotometer was used for determining emission spectra. Fluorescence quantum yields were determined by using Rhodamine 6G in ethanol (ϕ_f = 0.95) as a reference. An electrochemical workstation (CHI 660E instrument) was used to obtain cyclic voltammograms. A ferrocenium/ferrocene (Fc^+/Fc) redox system was used as an internal standard.

General Procedure for the Synthesis of Aldehydes 3 and 4. 4-Fluorobenzaldehyde (10 mmol) was added to a round-bottom flask. DMF (3.5 mL) was added to the flask, and then 22 mmol of piperidine (for **3**) or pyrrolidine (for **4**) was added to the reaction mixture, followed by the addition of potassium carbonate (20 mmol). The reaction mixture was heated at 140 °C for 20 h. Upon completion of the reaction, distilled water (100 mL) was added to the reaction flask. The mixture was transferred to a separating funnel and the product was extracted with DCM (3 × 30 mL). The crude product was then purified through column chromatography.

*4-(Piperidin-1-yl)benzaldehyde (**3**).* 93%; mp 62−63 °C; ^{1}H NMR (600 MHz, $CDCl_3$) δ: 9.76 (s, 1H), 7.74 (d, J = 8.5 Hz, 2H), 6.99 (s, 2H), 3.41 (t, J = 5.5 Hz, 4H), 1.94−1.43 (m, 6H) matches with;[50] IR (cm^{-1}) ATR 1662; MS m/z [M^+], 189.10.

*4-(Pyrrolidin-1-yl)benzaldehyde (**4**).* 97%; mp 88−90 °C; ^{1}H NMR ($CDCl_3$, 600 MHz) δ: 9.71 (1H, s), 7.72 (2H, d, J = 8.5 Hz), 6.61 (2H, d, J = 8.4 Hz), 3.42−3.36 (4H, m), 2.09−2.00 (4H, m) matches with;[51] IR (cm^{-1}) ATR 1651; MS m/z [M^+], 175.07.

General Procedure for the Synthesis of Chalcones 7 and 8. An appropriate amount of benzaldehyde (1 mmol) was added to ethanol (2 mL) in a round-bottom flask. Acetophenone (1 mmol) was added to the reaction flask.

https://doi.org/10.1021/acsomega.3c02813
ACS Omega 2023, 8, 28499−28510

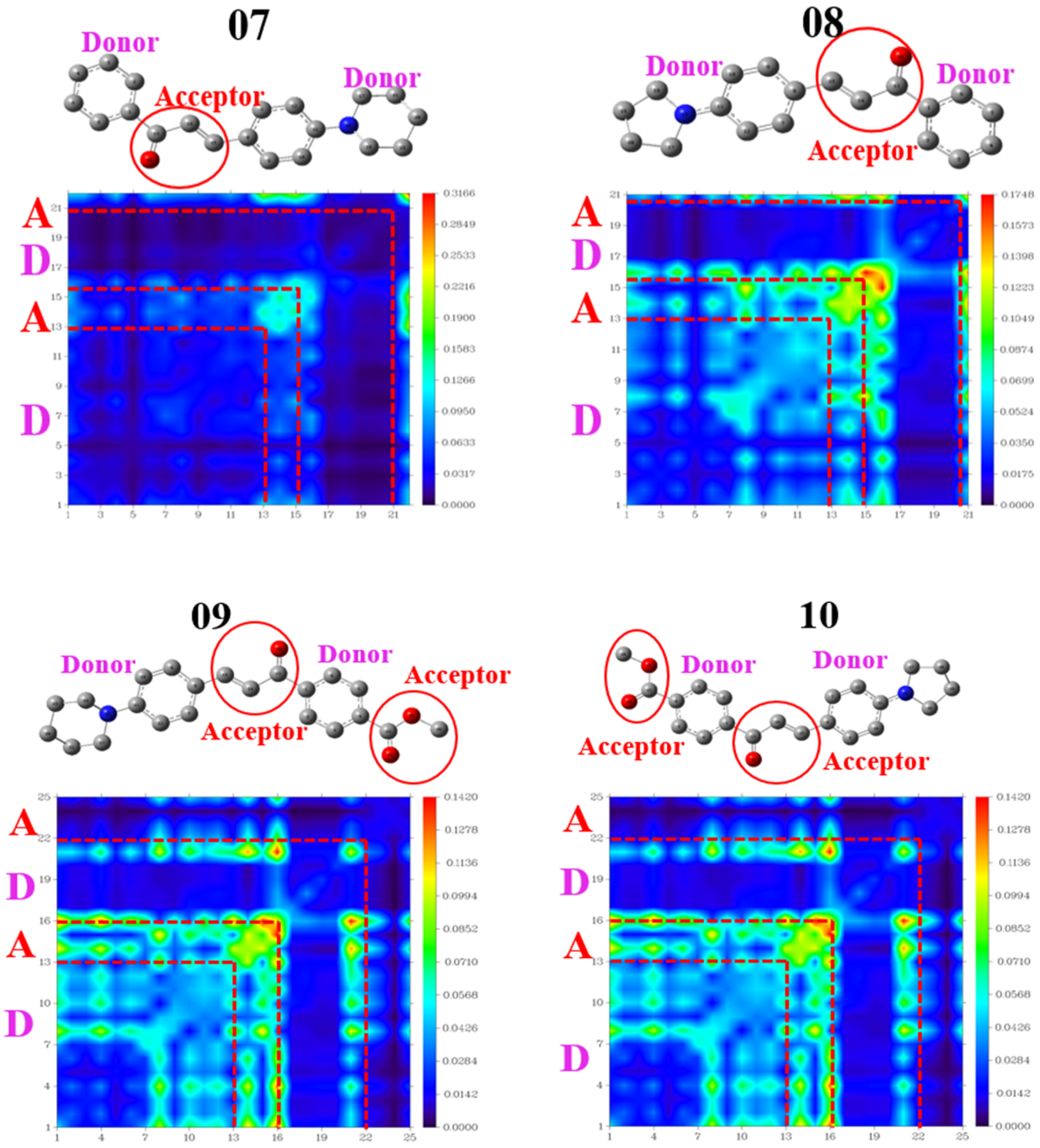

Figure 8. TDM graphs of chalcones **7**−**10**.

Table 7. Computed Charge-Transfer Integral Values of Chalcones 7−10

molecules	t_e (eV)	t_h (eV)
7	0.70	0.54
8	0.71	0.58
9	0.53	0.58
10	0.53	0.61

Table 8. Computed Dipole Moment of Chalcones 7−10 in the Ground State (μg) and Excited State (μe)

molecules	μ_g (D)	μ_e (D)
7	6.89	9.95
8	4.63	8.56
9	6.33	7.82
10	6.74	11.27

https://doi.org/10.1021/acsomega.3c02813
ACS Omega 2023, 8, 28499−28510

Sodium hydroxide (100 mg, 2.5 mmole) was dissolved in distilled water (1 mL) and added to the reaction mixture in a dropwise manner. The mixture was then stirred at room temperature for 15−17 h. At the completion of the reaction, the mixture was placed in an ice bath and neutralized with HCl. The ppt formed was collected and washed with cold ethanol. The purification of the crude product was done using column chromatography.

*(E)-1-Phenyl-3-(4-(piperidin-1-yl)phenyl)prop-2-en-1-one (**7**).* 66%; mp 131−134 °C; ^{1}H NMR ($CDCl_3$, 600 MHz) δ: 8.03−7.98 (2H, m), 7.77 (1H, d, J = 15.5 Hz), 7.60−7.53 (3H, m), 7.49 (2H, dd, J = 8.3, 6.9 Hz), 7.37 (1H, d, J = 15.5 Hz), 6.95 (1H, s), 3.35−3.30 (4H, m), 1.68 (6H, d, J = 48.1 Hz); ^{13}C NMR (151 MHz, $CDCl_3$) δ: 190.8, 153.2, 145.4, 139.0, 132.4, 130.4, 128.6, 128.5, 124.6, 118.2, 115.1, 49.3, 25.4, 24.3; IR (cm^{-1}) ATR 1648, 1556, 1122; MS m/z [M^+] 291.08; HRMS calcd for $C_{20}H_{21}NNaO^+$, 314.1515 [M + H]$^+$ found, 314.1517.

*(E)-1-Phenyl-3-(4-(pyrrolidin-1-yl)phenyl)prop-2-en-1-one (**8**).* 56%; mp 174−176 °C; ^{1}H NMR ($CDCl_3$, 600 MHz) δ: 7.55 (3H, t, J = 7.5 Hz), 7.48 (2H, t, J = 7.6 Hz), 7.33 (1H, d, J = 15.5 Hz), 6.63 (2H, d, J = 8.3 Hz), 3.41−3.36 (4H, m), 2.11−2.01 (4H, m); ^{13}C NMR (151 MHz, DMSO) δ: 190.8, 149.4, 146.1, 139.3, 132.2, 130.7, 128.6, 128.4, 123.0, 116.9, 112.5, 48.3, 25.6; IR (cm^{-1}) ATR 1643,1159; MS m/z [M^+] 277.09; HRMS calcd for $C_{19}H_{20}NO^+$, 278.1539 [M + H]$^+$ found, 278.1532.

General Procedure for the Synthesis of Chalcones 9 and 10. Methyl 4-acetylbenzoate (2 mmol) was added to a reaction flask, and dioxane (2 mL) was added to the reaction. Then, an appropriate amount of benzaldehyde (2.2 mmol) was added to the reaction flask, followed by the addition of piperidine (0.5 mL). The mixture was then refluxed for 24 h. Upon completion of the reaction, the mixture was allowed to cool down. The product was then obtained via column chromatography.

*Methyl (E)-4-(3-(4-(Piperidin-1-yl)phenyl)acryloyl)-benzoate (**9**).* 45%; mp 158−161 °C; ^{1}H NMR (DMSO, 600 MHz) δ: 8.21 (2H, d, J = 8.3 Hz), 8.09 (2H, d, J = 8.2 Hz), 7.85−7.53 (4H, m), 6.96 (2H, d, J = 8.6 Hz), 3.90 (3H, s), 3.34 (4H, m), 1.59 (6H, s); ^{13}C NMR (151 MHz, DMSO) δ: 188.3, 165.7, 152.8, 145.7, 141.9, 132.6, 131.0, 129.4, 128.5, 123.2, 116.7, 114.1, 52.4, 48.0, 24.9, 24.0; IR (cm^{-1}) ATR 1729, 1649, 1276; MS m/z [M^+] 349.14; HRMS calcd for $C_{22}H_{24}NO_3^+$, 350.1751 [M + H]$^+$ found, 350.1755;

*Methyl (E)-4-(3-(4-(Pyrrolidin-1-yl)phenyl)acryloyl)-benzoate (**10**).* 68%; mp 190−194 °C; ^{1}H NMR ($CDCl_3$, 600 MHz) δ: 8.14 (2H, d, J = 8.0 Hz), 8.03 (2H, d, J = 8.0 Hz), 7.80 (1H, d, J = 15.4 Hz), 7.56 (2H, d, J = 8.4 Hz), 7.29 (1H, d, J = 15.4 Hz), 3.96 (3H, s), 3.42−3.35 (4H, m), 2.11−2.03 (4H, m); ^{13}C NMR (151 MHz, DMSO) δ: 188.1, 165.7, 149.7, 146.5, 142.1, 132.5, 131.3, 129.4, 128.4, 121.3, 115.2, 111.8, 52.4, 47.3, 24.9; IR (cm^{-1}) ATR 1723, 1641, 1258; MS m/z [M^+] 335.03; HRMS calcd for $C_{21}H_{22}NO_3^+$, 336.1594 [M + H]$^+$ found, 336.1595.

UV−Visible Analysis. The photophysical studies of compounds **07−10** were carried out in spectroscopic grade solvents (acetonitrile, chloroform, and ethanol) at a concentration of 1 × 10^{-5} M. The UV−vis spectra of all compounds were recorded with a SHIMADZU UV-1800 spectrophotometer with the wavelength range from 200 to 800 nm using glass cuvettes with a path length of 1 cm.

PL and Fluorescence Quantum Yield (φ_f). The emission spectra of all the synthesized compounds were recorded on a Perkin Elmer multimode spectrophotometer at a concentration of 1 × 10^{-5} M at their excitation wavelength.

The fluorescence quantum yield (φ_f) was determined using a standard comparative method relative to standard Rhodamine 6G (φ_f = 0.91, chloroform[52]) by using the following relationship.

$$\varphi_f = \varphi_{f(s)} \frac{\mathrm{Grad}_u n_u^2}{\mathrm{Grad}_s n_s^2}$$

where φ_f is the fluorescence quantum yield. Grad = gradient of the plot of the integrated area under the curve of the emission spectra of unknown and standard. n = refractive indices of solvents. Subscripts "s" and "u" refer to the standard and unknown fluorophores, respectively.

Standard solutions of various concentrations of compounds **07−10** and rhodamine 6G were prepared in chloroform and ethanol, respectively, with an absorbance of less than 0.1. The emission spectra of these solutions were recorded at their excitation wavelengths of 405, 423, 420, 440, and 518 nm, respectively, to calculate integrated fluorescence intensity (peak area). Then, a plot was drawn by taking absorbance along the x-axis and the integrated area of fluorescence spectra along the y-axis. The slope of the straight line was used as the gradient in the above-mentioned equation. The value of factor $(n_u/n_s)^2$ was calculated by putting the refractive index value of chloroform for the unknown and ethanol for the standard. Thus, by substituting the values of gradients and refractive indices of unknown and standard and φ_f of standard in the above-mentioned equation, fluorescence quantum yields were calculated.

Cyclic Voltammetry (CV). The electrochemical analysis was performed on a CHI 660E workstation at room temperature by using a three-electrode cell system in a solution of tetrabutylammonium hexafluorophosphate (nBu_4NPF_6) 0.1 M as a supporting electrolyte in anhydrous acetonitrile at a scan rate of 100 mV s^{-1} between voltage ranges −1.5 and 1.5 V. The glassy carbon electrode was used as the working electrode, the Pt wire was used as the counter electrode, and the Ag/AgCl electrode was used as the reference electrode. The surface of the working electrode was cleaned after each scan by mechanical polishing using alumina slurry.

The highest occupied molecular orbital energy was calculated by using the following empirical equation.

$$E_{\mathrm{HOMO}} = -(E_{\mathrm{onset}} - E_{\mathrm{FC/FC+}} + 4.8)\mathrm{eV}$$

where E_{onset} is the onset of the corresponding oxidation potential peak. $E_{FC/FC+}$ is the onset of the oxidation potential peak of the ferrocene/ferrocenium redox couple used as a reference.

The lowest unoccupied molecular orbital energy was calculated by using the following relation.

$$E_{\mathrm{LUMO}} = E_{\mathrm{HOMO}} - E_{0-0}$$

where E_{0-0} is the optical band gap calculated by using the formula $1240/\lambda_{\mathrm{onset}}$, where λ_{onset} is the long edge of absorption spectra.

Computational Methodology. The Gaussian 09 software package was employed for the theoretical study of the compounds, and the Gauss View 5.0.8 program was used for presenting the findings. DFT was used to calculate electronic,

https://doi.org/10.1021/acsomega.3c02813
ACS Omega 2023, 8, 28499−28510

spectroscopic, and thermodynamic parameters. The energy calculations of the excited state were performed for calculating λ_{max} in the solvent (chloroform) and the gaseous phase. After processing data through SWizard software, the UV−vis absorption spectra were plotted using the Origin 6.0 program. To investigate the role of each fragment in charge transfer, the DOS was computed with PyMOlyze 1.1 software. To assess exciton excitation processes, the TDM was estimated and plotted with the Multiwfn 3.7 package.

■ ASSOCIATED CONTENT

Supporting Information

The Supporting Information is available free of charge at https://pubs.acs.org/doi/10.1021/acsomega.3c02813.

NMR and HRMS spectra and graphs used for calculating φ_f can be downloaded from the publisher's website (PDF)

■ AUTHOR INFORMATION

Corresponding Author

Rahman Shah Zaib Saleem − *Department of Chemistry and Chemical Engineering, Syed Babar Ali School of Science and Engineering, Lahore University of Management Sciences, Lahore 54792, Pakistan;* orcid.org/0000-0002-9615-4471; Phone: +92-42-3560-8215; Email: rahman.saleem@lums.edu.pk

Authors

Humera Baig − *Department of Chemistry and Chemical Engineering, Syed Babar Ali School of Science and Engineering, Lahore University of Management Sciences, Lahore 54792, Pakistan;* orcid.org/0000-0002-8550-9775

Amber Iqbal − *Department of Chemistry and Chemical Engineering, Syed Babar Ali School of Science and Engineering, Lahore University of Management Sciences, Lahore 54792, Pakistan*

Alvina Rasool − *Department of Chemistry, University of Agriculture, Faisalabad 38000, Pakistan*

Syed Zajif Hussain − *Department of Chemistry and Chemical Engineering, Syed Babar Ali School of Science and Engineering, Lahore University of Management Sciences, Lahore 54792, Pakistan;* orcid.org/0000-0002-3834-6061

Javed Iqbal − *Department of Chemistry, University of Agriculture, Faisalabad 38000, Pakistan*

Meshari Alazmi − *College of Computer Science and Engineering, University of Ha'il, Ha'il 81481, Saudi Arabia*

Nawaf Alshammari − *College of Sciences, University of Ha'il, Ha'il 81481, Saudi Arabia*

Amira Alazmi − *Department of Science and Technology, University Colleges at Nairiyah, University of Hafr Al Batin, Nairiyah 31981, Saudi Arabia*

Amer AlGhadhban − *College of Engineering, University of Ha'il, Ha'il 81481, Saudi Arabia*

Abdel Moneim E. Sulieman − *College of Sciences, University of Ha'il, Ha'il 81481, Saudi Arabia*

Kamaleldin B. Said − *Department of Pathology and Microbiology, College of Medicine, University of Ha'il, Ha'il 55476, Saudi Arabia*

Habib-ur Rehman − *Department of Chemistry and Chemical Engineering, Syed Babar Ali School of Science and Engineering, Lahore University of Management Sciences, Lahore 54792, Pakistan;* orcid.org/0000-0003-3407-5986

Complete contact information is available at: https://pubs.acs.org/10.1021/acsomega.3c02813

Notes

The authors declare no competing financial interest.

■ ACKNOWLEDGMENTS

This research has been funded by Scientific Research Deanship at the University of Ha'il—Saudi Arabia through project number RG-21 024.

■ REFERENCES

(1) Tang, C. W.; VanSlyke, S. A. Organic electroluminescent diodes. *Appl. Phys. Lett.* **1987**, *51*, 913−915.

(2) Jadhav, T.; Maragani, R.; Misra, R.; Sreeramulu, V.; Rao, D. N.; Mobin, S. M. Design and synthesis of donor-acceptor pyrazabole derivatives for multiphoton absorption. *Dalton Trans.* **2013**, *42*, 4340−4342.

(3) Maragani, R.; Misra, R.; Roy, M. S.; Singh, M. K.; Sharma, G. D. (D−π−A)$_2$−π−D−A type ferrocenyl bisthiazole linked triphenylamine based molecular systems for DSSC: synthesis, experimental and theoretical performance studies. *Phys. Chem. Chem. Phys.* **2017**, *19*, 8925−8933.

(4) Kukhta, N. A.; Bryce, M. R. Dual emission in purely organic materials for optoelectronic applications. *Mater. Horiz.* **2021**, *8*, 33−55.

(5) Gierschner, J.; Shi, J.; Milián-Medina, B.; Roca-Sanjuán, D.; Varghese, S.; Park, S. Luminescence in Crystalline Organic Materials: From Molecules to Molecular Solids. *Adv. Opt. Mater.* **2021**, *9*, 2002251.

(6) Zhu, M.; Yang, C. Blue fluorescent emitters: design tactics and applications in organic light-emitting diodes. *Chem. Soc. Rev.* **2013**, *42*, 4963−4976.

(7) Gu, P. Y.; Zhao, Y.; He, J. H.; Zhang, J.; Wang, C.; Xu, Q. F.; Lu, J. M.; Sun, X. W.; Zhang, Q. Synthesis, Physical Properties, and Light-Emitting Diode Performance of Phenazine-Based Derivatives with Three, Five, and Nine Fused Six-Membered Rings. *J. Org. Chem.* **2015**, *80*, 3030−3035.

(8) Zhang, Q.; Divayana, Y.; Xiao, J.; Wang, Z.; Tiekink, E. R. T.; Doung, H. M.; Zhang, H.; Boey, F.; Sun, X. W.; Wudl, F. Synthesis, Characterization, and Bipolar Transporting Behavior of a New Twisted Polycyclic Aromatic Hydrocarbon: 1′,4′-Diphenyl-naphtho-(2′.3′:1.2)-pyrene-6′-nitro-7′-methyl Carboxylate. *Chem.—Eur. J.* **2010**, *16*, 7422−7426.

(9) Xiao, J.; Yang, H.; Yin, Z.; Guo, J.; Boey, F.; Zhang, H.; Zhang, Q. Preparation, characterization, and photoswitching/light-emitting behaviors of coronene nanowires. *J. Mater. Chem.* **2011**, *21*, 1423−1427.

(10) Gonçalves, M. S. T. Fluorescent labeling of biomolecules with organic probes. *Chem. Rev.* **2009**, *109*, 190−212.

(11) Khan, F.; Misra, R. Recent advances in the development of phenothiazine and its fluorescent derivatives for optoelectronic applications. *J. Mater. Chem. C* **2023**, *11*, 2786−2825.

(12) Huang, X.; Han, S.; Huang, W.; Liu, X. Enhancing solar cell efficiency: the search for luminescent materials as spectral converters. *Chem. Soc. Rev.* **2013**, *42*, 173−201.

(13) Kaur, N.; Singh, M.; Pathak, D.; Wagner, T.; Nunzi, J. M. Organic materials for photovoltaic applications: Review and mechanism. *Synth. Met.* **2014**, *190*, 20−26.

(14) Liu, Z.; Qi, W.; Xu, G. Recent advances in electrochemiluminescence. *Chem. Soc. Rev.* **2015**, *44*, 3117−3142.

(15) Chou, Y.-H.; Tsai, C.-L.; Chen, W.-C.; Liou, G.-S. Nonvolatile transistor memory devices based on high-k electrets of polyimide/TiO 2 hybrids. *Polym. Chem.* **2014**, *5*, 6718−6727.

(16) Li, G.; Wu, Y.; Gao, J.; Li, J.; Zhao, Y.; Zhang, Q. Synthesis, Physical Properties, and Anion Recognition of Two Novel Larger Azaacenes: Benzannelated Hexazaheptacene and Benzannelated N,N′-Dihydrohexazaheptacene. *Chem.—Asian J.* **2013**, *8*, 1574−1578.
(17) Ibnaouf, K.; Elzupir, A.; AlSalhi, M.; Alaamer, A. S. Influence of functional groups on the photophysical properties of dimethylamino chalcones as laser dyes. *Opt. Mater.* **2018**, *76*, 216−221.
(18) Gao, Z.; Hao, Y.; Zheng, M.; Chen, Y. A fluorescent dye with large Stokes shift and high stability: synthesis and application to live cell imaging. *RSC Adv.* **2017**, *7*, 7604−7609.
(19) Espinoza-Hicks, J.; Nápoles-Duarte, J.; Nevárez-Moorillón, G.; Camacho-Dávila, A.; Rodríguez-Valdez, L. Synthesis, electronic, and spectral properties of novel geranylated chalcone derivatives: a theoretical and experimental study. *J. Mol. Model.* **2016**, *22*, 253−313.
(20) da Costa, R. G. M.; de Queiroz Garcia, R.; Fiuza, R. M. d. R.; Maqueira, L.; Pazini, A.; De Boni, L.; Limberger, J. Synthesis, photophysical properties and aggregation-induced enhanced emission of bischalcone-benzothiadiazole and chalcone-benzothiadiazole hybrids. *J. Lumin.* **2021**, *239*, 118367.
(21) Irfan, R.; Mousavi, S.; Alazmi, M.; Saleem, R. S. Z. A comprehensive review of aminochalcones. *Molecules* **2020**, *25*, 5381.
(22) Zhuang, C.; Zhang, W.; Sheng, C.; Zhang, W.; Xing, C.; Miao, Z. Chalcone: a privileged structure in medicinal chemistry. *Chem. Rev.* **2017**, *117*, 7762−7810.
(23) Karthikeyan, C.; Narayana Moorthy, N. S.; Ramasamy, S.; Vanam, U.; Manivannan, E.; Karunagaran, D.; Trivedi, P. Advances in chalcones with anticancer activities. *Recent Pat. Anti-Cancer Drug Discov.* **2014**, *10*, 97−115.
(24) Iftikhar, S.; Khan, S.; Bilal, A.; Manzoor, S.; Abdullah, M.; Emwas, A. H.; Sioud, S.; Gao, X.; Chotana, G. A.; Faisal, A.; et al. Synthesis and evaluation of modified chalcone based p53 stabilizing agents. *Bioorg. Med. Chem. Lett.* **2017**, *27*, 4101−4106.
(25) Riaz, S.; Iqbal, M.; Ullah, R.; Zahra, R.; Chotana, G. A.; Faisal, A.; Saleem, R. S. Z. Synthesis and evaluation of novel alpha-substituted chalcones with potent anti-cancer activities and ability to overcome multidrug resistance. *Bioorg. Chem.* **2019**, *87*, 123−135.
(26) Malik, H. S.; Bilal, A.; Ullah, R.; Iqbal, M.; Khan, S.; Ahmed, I.; Krohn, K.; Saleem, R. S. Z.; Hussain, H.; Faisal, A. Natural and Semisynthetic Chalcones as Dual FLT3 and Microtubule Polymerization Inhibitors. *J. Nat. Prod.* **2020**, *83*, 3111−3121.
(27) Won, S.-J.; Liu, C.-T.; Tsao, L.-T.; Weng, J.-R.; Ko, H.-H.; Wang, J.-P.; Lin, C.-N. Synthetic chalcones as potential anti-inflammatory and cancer chemopreventive agents. *Eur. J. Med. Chem.* **2005**, *40*, 103−112.
(28) Ritter, M.; Martins, R.; Dias, D.; MP Pereira, C. Recent advances on the synthesis of chalcones with antimicrobial activities: a brief review. *Lett. Org. Chem.* **2014**, *11*, 498−508.
(29) Xu, M.; Wu, P.; Shen, F.; Ji, J.; Rakesh, K. Chalcone derivatives and their antibacterial activities: Current development. *Bioorg. Chem.* **2019**, *91*, 103133.
(30) Borchhardt, D. M.; Mascarello, A.; Chiaradia, L. D.; Nunes, R. J.; Oliva, G.; Yunes, R. A.; Andricopulo, A. D. Biochemical evaluation of a series of synthetic chalcone and hydrazide derivatives as novel inhibitors of cruzain from Trypanosoma cruzi. *J. Braz. Chem. Soc.* **2010**, *21*, 142−150.
(31) Elkhalifa, D.; Al-Hashimi, I.; Al Moustafa, A. E.; Khalil, A. A comprehensive review on the antiviral activities of chalcones. *J. Drug Target.* **2021**, *29*, 403−419.
(32) Gacche, R. N.; Dhole, N. A.; Kamble, S. G.; Bandgar, B. P. In-vitro evaluation of selected chalcones for antioxidant activity. *J. Enzyme Inhib. Med. Chem.* **2008**, *23*, 28−31.
(33) Kyogoku, K.; Hatayama, K.; Yokomori, S.; Saziki, R.; Nakane, S.; Sasajima, M.; Sawada, J.; Ohzeki, M.; Tanaka, I. Anti-ulcer effect of isoprenyl flavonoids. II. Synthesis and anti-ulcer activity of new chalcones related to sophoradin. *Chem. Pharm. Bull.* **1979**, *27*, 2943−2953.
(34) Hayat, F.; Moseley, E.; Salahuddin, A.; Van Zyl, R. L.; Azam, A. Antiprotozoal activity of chloroquinoline based chalcones. *Eur. J. Med. Chem.* **2011**, *46*, 1897−1905.
(35) Rammohan, A.; Bhaskar, B. V.; Venkateswarlu, N.; Gu, W.; Zyryanov, G. V. Design, synthesis, docking and biological evaluation of chalcones as promising antidiabetic agents. *J. Braz. Chem. Soc.* **2020**, *95*, 103527.
(36) Ali, M.; Elzupir, A.; Ibrahem, M.; Suliman, I.; Modwi, A.; Idriss, H.; Ibnaouf, K. Characterization of optical and morphological properties of chalcone thin films for optoelectronics applications. *Optik* **2017**, *145*, 529−533.
(37) Sharma, V. S.; Sharma, A. S.; Agarwal, N. K.; Shah, P. A.; Shrivastav, P. S. Self-assembled blue-light emitting materials for their liquid crystalline and OLED applications: from a simple molecular design to supramolecular materials. *Mol. Syst. Des. Eng.* **2020**, *5*, 1691−1705.
(38) Fayed, T. A. A novel chalcone-analogue as an optical sensor based on ground and excited states intramolecular charge transfer: A combined experimental and theoretical study. *Chem. Phys.* **2006**, *324*, 631−638.
(39) Custodio, J. M.; Gotardo, F.; Vaz, W. F.; D'Oliveira, G. D.; de Almeida, L. R.; Fonseca, R. D.; Cocca, L. H.; Perez, C. N.; Oliver, A. G.; De Boni, L.; et al. Benzenesulfonyl incorporated chalcones: Synthesis, structural and optical properties. *J. Mol. Struct.* **2020**, *1208*, 127845.
(40) Anandkumar, D.; Ganesan, S.; Rajakumar, P.; Maruthamuthu, P. Synthesis, photophysical and electrochemical properties and DSSC applications of triphenylamine chalcone dendrimers via click chemistry. *New J. Chem.* **2017**, *41*, 11238−11249.
(41) Baig, H.; Irfan, R.; Rasool, A.; Hussain, S. Z.; Siddique, S. A.; Iqbal, J.; Alazmi, M.; Alshammari, N.; Alazmi, A.; AlGhadhban, A.; et al. Synthesis, photophysical, voltammetric, and DFT studies of 4-aminochalones. *J. Photochem. Photobiol., A* **2023**, *442*, 114790.
(42) Baig, H.; Rasool, A.; Hussain, S. Z.; Iqbal, J.; Ashraf, R. S.; Emwas, A.-H.; Alazmi, M.; Gao, X.; Chotana, G. A.; Saleem, R. S. Z.; et al. Synthesis, photophysical, electrochemical and computational studies of novel 2-aminoimidazolones with D-π-A framework. *J. Photochem. Photobiol., A* **2022**, *429*, 113918.
(43) Beerepoot, M. T.; Friese, D. H.; List, N. H.; Kongsted, J.; Ruud, K. Benchmarking two-photon absorption cross sections: performance of CC2 and CAM-B3LYP. *Phys. Chem. Chem. Phys.* **2015**, *17*, 19306−19314.
(44) Adamo, C.; Barone, V. Exchange functionals with improved long-range behavior and adiabatic connection methods without adjustable parameters: The m PW and m PW1PW models. *Chem. Phys. Lett.* **1998**, *108*, 664−675.
(45) Chai, J.-D.; Head-Gordon, M. Long-range corrected hybrid density functionals with damped atom−atom dispersion corrections. *Phys. Chem. Chem. Phys.* **2008**, *10*, 6615−6620.
(46) Finley, J. P. Using the local density approximation and the LYP, BLYP and B3LYP functionals within reference-state one-particle density-matrix theory. *Mol. Phys.* **2004**, *102*, 627−639.
(47) Rafiq, M.; Khera, R. A.; Salim, M.; Khalid, M.; Ayub, K.; Iqbal, J. Tuning the optoelectronic properties of scaffolds by using variable central core unit and their photovoltaic applications. *Chem. Phys. Lett.* **2021**, *782*, 139018.
(48) Ottonelli, M.; Piccardo, M.; Duce, D.; Thea, S.; Dellepiane, G. Koopmans' Transfer Integral Calculation: A Comparison between the Hartree-Fock and the Density Functional Results. *Energy Proc.* **2012**, *31*, 31−37.
(49) Zhang, L.; Shen, W.; He, R.; Liu, X.; Tang, X.; Yang, Y.; Li, M. Fine structural tuning of diketopyrrolopyrrole-cored donor materials for small molecule-fullerene organic solar cells: A theoretical study. *Org. Electron.* **2016**, *32*, 134−144.
(50) Yuan, C.; Zhang, L.; Zhao, Y. Cu(II)-Catalyzed C-N Coupling of (Hetero)aryl Halides and N-Nucleophiles Promoted by α-Benzoin Oxime. *Molecules* **2019**, *24*, 4177.
(51) Sarma, M.; Chatterjee, T.; Ghanta, S.; Das, S. K. D-π-A-A-π-D Prototype 2,2′-Bipyridine Dyads Exhibiting Large Structure and Environment-Sensitive Fluorescence: Synthesis, Photophysics, and Computation. *J. Org. Chem.* **2012**, *77*, 432−444.

https://doi.org/10.1021/acsomega.3c02813
ACS Omega 2023, 8, 28499−28510

(52) Ogunsipe, A. Solvent effects on the spectral properties of rhodamine 6g: Estimation of ground and excited state dipole moments. *J. Solution Chem.* **2018**, *47*, 203−219.

https://doi.org/10.1021/acsomega.3c02813
ACS Omega 2023, 8, 28499−28510